

Modeling cell migration regulated by cell-ECM micromechanical coupling

Yu Zheng*,¹ Hanqing Nan*,² Qihui Fan*,^{3,4} Xiaochen Wang,^{3,4} Liyu Liu,⁵ Ruchuan Liu,^{5,†} Fangfu Ye,^{3,4,‡} Bo Sun,^{6,§} and Yang Jiao^{2,1,¶}

¹Department of Physics, Arizona State University, Tempe, AZ 85287

²Materials Science and Engineering, Arizona State University, Tempe, AZ 85287

³Beijing National Laboratory for Condensed Matter Physics and CAS Key Laboratory of Soft Matter Physics, Institute of Physics, Chinese Academy of Sciences, Beijing 100190, China

⁴School of Physical Sciences, University of Chinese Academy of Sciences, Beijing 100049, China

⁵College of Physics, Chongqing University, Chongqing 401331, China

⁶Department of Physics, Oregon State University, Corvallis, OR 97331

Cell migration in fibrous extracellular matrix (ECM) is crucial to many physiological and pathological processes such as tissue regeneration, immune response and cancer progression. During migration, individual cells can generate active pulling forces via actin filament contraction, which are transmitted to the ECM fibers through focal adhesion complexes, remodel the ECM, and eventually propagate to and can be sensed by other cells in the system. The microstructure and physical properties of the ECM can also significantly influence cell migration, e.g., via durotaxis and contact guidance. Here, we develop a computational model for cell migration regulated by cell-ECM micro-mechanical coupling. Our model explicitly takes into account a variety of cellular level processes including focal adhesion formation and disassembly, active traction force generation and cell locomotion due to actin filament contraction, transmission and propagation of tensile forces in the ECM, as well as the resulting ECM remodeling. We validate our model by accurately reproducing single-cell dynamics of MCF-10A breast cancer cells migrating on collagen gels and show that the durotaxis and contact guidance effects naturally arise as a consequence of the cell-ECM micro-mechanical interactions considered in the model. Moreover, our model predicts strongly correlated multi-cellular migration dynamics, which are resulted from the ECM-mediated mechanical coupling among the migrating cell and are subsequently verified in *in vitro* experiments using MCF-10A cells. Our computational model provides a robust tool to investigate emergent collective dynamics of multi-cellular systems in complex *in vivo* micro-environment and can be utilized to design *in vitro* micro-environments to guide collective behaviors and self-organization of cells.

I. INTRODUCTION

Cell migration in fibrous extracellular matrix (ECM) is a complex dynamic process involving a series of intra-cellular and extra-cellular activities including the development of filopodia, formation of focal adhesion sites, locomotion due to actin filament contraction, and detachment of the rear end [5, 6]. Collective cell migration in a complex micro-environment is crucial to many physiological and pathological processes including tissue regeneration, immune response and cancer progression [1–4]. Besides the well-established chemotaxis [7], the microstructure and physical properties of the ECM can also significantly influence cell migration via durotaxis [8–10], haptotaxis [11], and contact guidance [12–14]. For example, in durotaxis, a cell can sense and respond to the rigidity gradient in the local micro-environment, which in turn guides its migration [10].

A migrating cell also generates active pulling forces [15], which are transmitted to the ECM fibers via focal

adhesion complexes [16–18]. Such active forces remodel the local ECM, e.g., by re-orienting the collagen fibers, forming fiber bundles and increasing the local stiffness of ECM [19–25]. Recent studies have indicated that a delicate balance among the magnitude of the pulling forces, the cell-ECM adhesion strength, and the ECM rigidity is required to achieve an optimal mode of single cell migration [26]. In a multi-cell system, the pulling forces generated by individual cells can give rise to a dynamically evolving force network (carried by the ECM fibers) in the system [27–31, 31–34]. In other words, the active pulling forces generated by individual cells can propagate in the ECM and can be sensed by distant cells. This ECM-mediated mechanical coupling among the cells could further influence the migration of the individual cells, which in turn alters the ECM structure and properties, and thus the tensile force network. This feedback loop between the force network and cell migration could lead to a rich spectrum of collective migratory behaviors.

A variety of computational models have been developed to investigate the migration dynamics of both single cell and multi-cellular systems [35–37] as well as various sub-cellular processes involved in cell migration [38–43]. For example, a migrating cell can be modelled as an “active particle” whose dynamics is mainly determined by an active self-propelling force, a random drift and various effective particle-particle and/or particle-environment interactions [44, 45]. A wide spectrum of collective dynam-

*These authors contributed equally to this work.

†correspondence sent to: phyliurc@cqu.edu.cn

‡correspondence sent to: fye@iphy.ac.cn

§correspondence sent to: sunb@physics.oregonstate.edu

¶correspondence sent to: yang.jiao.2@asu.edu

ics have been observed and investigated in active-particle systems [45]. On the other hand, vertex-based models [46] and multi-state cellular Potts models [47] are usually employed to investigate the collective dynamics of densely packed sheets of cells, including the spontaneous cell sorting driven by differential adhesion and the epithelial to mesenchymal transition (EMT). Recently, cellular automaton models which explicitly consider the migration of invasive tumor cells following least-resistance paths have been devised to study the emergence of invasive dendritic structures composed of highly malignant tumor cells emanating from the primary tumor mass [48–51].

In the preponderance of existing cell migration models, the influence of the cell-ECM interactions and/or ECM-mediated indirect cell-cell interactions on collective migration dynamics either is not considered or is incorporated in an effective phenomenological manner. Recently, a computational model based on continuum mechanics has been developed that explicitly considers the micro-mechanical coupling of a migrating cell and the 2D substrate [52]. Durotaxis effects have been successfully reproduced from this model. Moreover, a novel model for investigating cell migration in model 2D ECM network guided by mechanical cues has been developed by considering coarse-grained cytoskeleton of a migrating cell as a part of the ECM network and the cells can hop between neighboring nodes of the network [53]. Even in these novel models which explicitly take into account cell-ECM micro-mechanical couplings, a number of processes crucial to cell migratory behaviors such as focal adhesion formation and disassembly, actin filament contraction and the resulting continuous cell locomotion, the remodeling of ECM network and the influence of the complex microstructure and topology of ECM network have not been explicitly considered and incorporated into the models.

Here, we develop a computational model for cell migration regulated by cell-ECM micro-mechanical coupling, which could be employed to investigate collective migratory behaviors and emergent self-organizing multicellular patterns resulted from ECM-mediated mechanical signaling among the cells. Our model takes into account a variety of cellular level processes including focal adhesion formation and disassembly, active traction force generation and cell locomotion due to actin filament contraction, transmission and propagation of tensile forces in the ECM. We employ a node-bond (i.e., graph) representation to model the complex 3D ECM network microstructure, which is reconstructed based on confocal imaging data. In addition, we use a nonlinear mechanical model for the ECM networks, which incorporates buckling of collagen fibers upon compression and strain-hardening upon stretching. We validate our model by accurately reproducing single-cell dynamics of MCF-10A breast cancer cells migrating on collagen gels and show that the durotaxis and contact guidance effects naturally arise as a consequence of the cell-ECM

micro-mechanical interactions considered in the model. Moreover, our model predicts strongly correlated multicellular migration dynamics, which are resulted from the ECM-mediated mechanical coupling among the migrating cell and are subsequently verified in *in vitro* experiments using MCF-10A cells.

The rest of the paper is organized as follows: In Sec. II, we describe the microstructural and mechanical model of the 3D ECM (mainly collagen I) networks. In Sec. III, we introduce our cell migration model and discuss the associated assumptions and limitations. In Sec. IV, we validate our model by producing single-cell migration dynamics of MCF-10A breast cancer cells on isotropic collagen network and investigate the cell migration dynamics on heterogeneous networks with stiffness gradient and aligned fibers. In Sec. V, we investigate collective multicellular dynamics resulted from ECM-mediated mechanical coupling among the migrating cells, and validate our results via *in vitro* experiments. In Sec. VI, we provide concluding remarks.

II. MICROSTRUCTURE AND MECHANICAL MODEL OF 3D ECM NETWORK

A. Modeling ECM Network via Statistical Descriptors and Stochastic Reconstruction

In this section, we briefly describe the microstructural and micro-mechanical models for the ECM networks. The detailed descriptions of these models are provided in Refs. [54] and [34], respectively. The 3D ECM, mainly composed of collagen type I gel, is modeled as a discrete network with a “graph” (i.e., node-bond) representation in a cubic simulation domain with linear size L ($\sim 300\mu\text{m}$), which is composed of M_n nodes and M_b bonds, depending on the collagen concentration. The average coordination number Z , i.e., the average number of bonds connected to each node, is given by $Z = 2M_b/M_n$. We mainly use fixed boundary (FB) conditions (i.e., the nodes within a certain distance $\delta L \sim 5\mu\text{m}$ from the boundaries of the simulation domain are fixed) in our simulations, but also confirm that using periodic boundary (PB) conditions does not affect the results for the large L values used in our simulations.

We employ a set of statistical descriptors for quantifying the network geometry and topology [54], which include the node density ρ (corresponding to the collagen concentration), the fiber (or bond) length distribution function P_f , the distribution of coordination number (i.e., the number of neighbors of a node) P_Z , and the average fiber orientation Ω (measured as the average cosine value associated with the acute angle of a fiber made with respect to a prescribed direction). These statistical descriptors can be computed from 3D ECM network extracted from confocal images via skeletonization techniques [20]. Fig. 1(c) and (d) respectively shows the coordination distribution P_Z and fiber length dis-

tribution P_f for homogeneous collagen networks with a collagen concentration of 2mg/ml , which will be used in our subsequent investigations. The average fiber length is $1.96\mu\text{m}$ and the average coordination number $Z = 3.4$. Since the fibers are randomly oriented in homogeneous networks, the average fiber orientation metric $\Omega \approx 0.5$. The node number density $\rho \approx 0.185/\mu\text{m}^3$.

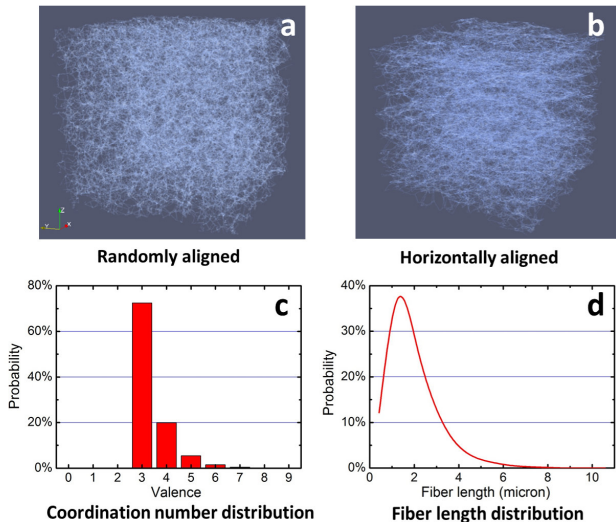


FIG. 1: Realizations of 3D ECM networks with randomly oriented fibers with $\Omega = 0.5$ (a) and horizontally aligned fibers with $\Omega = 0.88$ (b), generated using stochastic reconstruction techniques. For better visualization, only small sub-networks with a linear size of $50\mu\text{m}$ are shown here. (c) and (d) respectively shows the coordination distribution P_Z and fiber length distribution P_f for the networks, which are computed based on confocal images of a 2 mg/ml collagen gel.

For a given set of network statistics (e.g., P_Z^* , P_f^* , Ω^* and ρ^*), we can generate realizations of the networks associated with the prescribed descriptors using stochastic reconstruction [54]. In particular, we start from a randomly generated initial network with the prescribed node number density ρ^* . From this initial network, the descriptors P_f , P_Z , and Ω are computed and compared to the corresponding prescribed descriptors. An energy functional E is defined as the sum of the squared differences between the computed and corresponding prescribed descriptors [54], i.e.,

$$E = \sum_r |P_Z(r) - P_Z^*(r)|^2 + \sum_r |P_f(r) - P_f^*(r)|^2 + |\Omega - \Omega^*|^2. \quad (1)$$

Next, the initial network is perturbed by randomly displacing a node and/or removing/adding a bond to randomly selected pairs of nodes. A new energy for the new network is computed. If the new energy E_{new} is lower than the old energy E_{old} , the new network replaces the old one. Otherwise, the new network configuration replaces the old network with the probability

$e^{(E_{old} - E_{new})/T}$, where T is a virtual temperature, which possesses an initial large value and is gradually decreased. The network is continuously evolved in this way (more precisely, via simulated annealing method [55] to allow even energy-increasing network during the initial stages) until $E \approx 0$, i.e., the computed descriptors match the prescribed ones within a prescribed small tolerance. The detailed of this technique is provided in Ref. [54].

We note that one can either use experimentally obtained network statistics as the target descriptors in the reconstruction or can construct a set of feasible hypothetical statistical descriptors in order to control the geometry and topology of the constructed random network. Fig. 1(a) shows a reconstructed network based on the experimentally obtained statistics of the 2mg/ml collagen gels, in which the fibers are randomly oriented. In order to investigate the effects of fiber alignment on cell migration dynamics, we also generate realizations of networks with horizontally aligned fibers (see Fig. 1(b)). This is achieved by setting $\Omega^* = 1$ with respect to the x-direction, and using the same P_Z^* , P_f^* and ρ^* of the homogeneous network. We note that the optimized Ω of the reconstructed network is in fact a little smaller than unity ($\Omega \sim 0.88$), due to additional topological and geometrical constraints specified by P_Z^* and P_f^* . Nevertheless, the fiber alignment is already very significant in the reconstructed networks.

B. Micro-mechanical Model of ECM Networks

The ECM (collagen) fibers are highly non-linear, typically exhibiting buckling, strain-hardening and plastic behaviors [20, 56–58], which can significantly affect the propagation of the active forces in the system. The non-linearity of the ECM fibers also induces a nontrivial coupling with the cell contractility, i.e., for small contraction, the fibers may be in the linear elastic regime, while for large contraction, the fibers may be in the strain-hardening or plastic regime [34]. This in turn can affect the overall cell migration dynamics [26].

In this work, we will use a nonlinear micromechanical model for the ECM fiber, which is schematically illustrated in Fig. 2 [34, 58]. In particular, upon stretching, a fiber first enters a linear elastic regime, which is followed by a strong strain-hardening regime once the elongation is larger than a prescribed threshold. Upon compression, we consider the fiber immediately buckles and thus, possesses a much smaller compression modulus. The elongation stiffness k of the fiber is thus given by

$$k = \begin{cases} \rho EA, & \lambda < 0 \\ EA, & 0 < \lambda < \lambda_s \\ EA \exp[(\lambda - \lambda_s)/\lambda_0], & \lambda > \lambda_s. \end{cases} \quad (2)$$

where E and A are respectively the Young's modulus

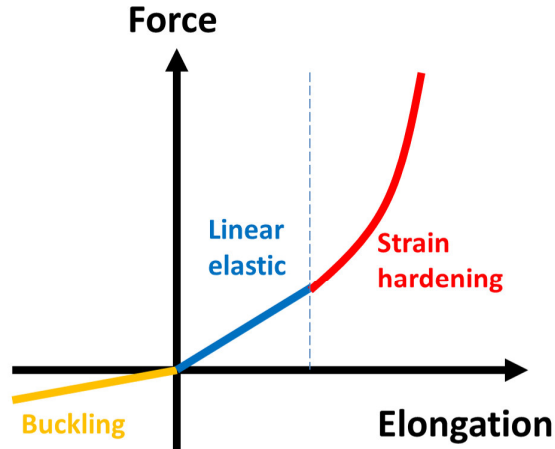


FIG. 2: Schematic illustration of the nonlinear elastic fiber model, including a linear elastic regime, which is followed by a strong strain-hardening regime upon compression and buckling upon compression.

and cross-sectional area of the fiber bundle, and we use $EA = 8 \times 10^{-7} N$ [20]; $\lambda = \delta\ell/\ell$ is elongation strain, and $\lambda_s = 0.02$ and $\lambda_0 = 0.05$ are parameters for the strain-hardening model [58]; $\rho = 0.1$ describes the effects of buckling [34]. In addition, we consider the fiber segments as well as the cross links (nodes) can resist bending and employ a first-order bending approximation [27], for which the bending energy E_b is a function of transverse displacement u of the two nodes of a fiber, i.e., $E_b = \alpha EI u^2 / \ell_0$, where the bending modulus $EI = 5 \times 10^{-22} Nm^2$ [20], I is the second moment of area, ℓ_0 is the original length of the fiber segment, and $\alpha = 1.8$. We also note that the effects of interstitial fluid, which quickly dissipates the kinetic energy generated due to cell contraction, are not explicitly considered.

Plasticity of the fibers is modeled as a time-dependent elongation of the fiber with a constant flow rate γ , i.e., $\delta l_P = \gamma t$, once the stretching force on the fiber is larger than a prescribed threshold f_P . The flow rate can be calibrated based on experimental data available in literature [24]. We note that this elongation due to plasticity effectively reduces the stiffness of the fiber, i.e., $k = EA / (l + \delta l_P)$. In addition, we can easily construct a stiffness gradient in the ECM network, by introducing a position-dependent scaling factor, i.e., $E(x) = E \cdot C_0(x)$, where $C_0(x) = (1 + x/L)$. It is clear that other forms of $C_0(x)$ than the simple linear scaling could be employed to model more stiffness gradient. In the subsequent studies, we will use the simple constant gradient to investigate the durotaxis effects.

Once the cell contractions are applied (as described in Sec. III), an iteration procedure [34] will be employed to find the force-balanced state of the network and obtain the forces on the fibers. The numerical procedure can be easily parallelized using OpenMP for large networks.

III. MODELING CELL MIGRATION REGULATED BY CELL-ECM MICRO-MECHANICAL COUPLING

In this section, we present in detail the cell migration model, which is coupled with the ECM network model. We note that the current model is targeted for highly motile non-invasive cancer cells, such as the MCF-10A breast cancer cells, moving on 3D collagen gel (see Fig. 3 for illustration). In this case, the migrating cells are strongly coupled with the ECM via their micro-mechanical interactions without any ECM degradation, which is very challenging to accurately model. We will briefly discuss the generalization of the current model to incorporate ECM degradation in Sec. VI.

As illustrated in Fig. 3, our cell model consists of an elastic sphere representing the exclusion volume associated with cytoplasm and a set of cytoskeleton filaments connecting the cytoplasm sphere to the plasma membrane. As a starting point, we will not distinguish various types of actin assemblies and microtubules for simplicity, and only consider the contractility of the filaments. The plasma membrane is then modeled as the minimal hull associated with the end points of the filaments (see Fig. 3(A)). In the beginning of the simulation, a cell (i.e., a cytoplasm sphere and the associated cytoskeleton filaments) is introduced in the collagen network, and a random persistent direction \mathbf{n}_0 is selected. The migration process is decomposed into cycles of successive events including (i) development of protrusion (due to active actin filaments polymerization) and formation of new adhesion sites, (ii) contraction of actin filaments and the resulting locomotion of the cell, and (iii) breaking of old adhesion sites. These events are modeled and simulated as described below:

- (i) Protrusions are generated by the elongation (polymerization) of the actin filaments, which can be attached to the ECM fibers via focal adhesion. This process is modeled by adding new filaments connecting the center of mass of the cell (i.e., the center of the cytoplasm sphere) to a randomly selected node of the ECM network within $\delta R_s \sim 5\mu m$ (effective protrusion length) from the cell surface (see Fig. 3(a) and (b)), with the probability p_a given by

$$p_a = c_1(\mathbf{n}_0 \cdot \mathbf{d}) + c_2\sigma_f \quad (3)$$

where \mathbf{n}_0 is the persistent direction of the cell, \mathbf{d} is vector connecting the cell center and the network node, σ_f is the largest stress on the fibers connected to the node, c_1 and c_2 are proportionality constants. This model implies that actin polymerization is more likely to occur in the polarized region of the cell [59]; and that it is more likely to form an adhesion site on highly stressed fibers [60, 61]. Each adhesion site has a finite life span T_a and breaks once T_a is reached.

- (ii) The contraction of an actin filament connecting the cytoplasm sphere and ECM network can generate a traction force \mathbf{f}_i ($\sim 1nN$) along the filament [62–65]

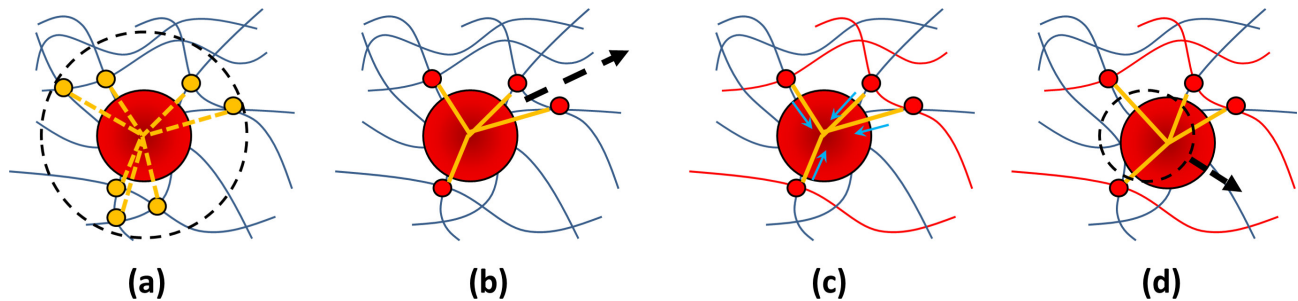


FIG. 3: Schematic illustration of the computational model for a migrating cell. (a) Protrusions (yellow dashed lines) generated by polymerization of actin filaments can lead to focal adhesion formation (yellow dots) in a region within δR_s (effective protrusion length) from the cell surface (region enclosed by dashed circle). (b) New focal adhesion (red dots) formation is modeled by adding new filaments (yellow solid lines) connecting the center of mass of the cell (i.e., the center of the cytoplasm sphere) to a randomly selected node of the ECM network within δR_s from the cell surface, with a probability depending on the persistent direction of the cell (dashed arrow) and the local stress state of the fibers. (c) Active contraction of actin filaments generates active forces in the ECM network and leads to deformation of ECM. (d) Locomotion of the cell due to actin filament contraction.

and a shrinkage of the filament length δl ($\sim 10\%$ of the original length); see Fig. 3(c). This active force is transmitted to the ECM network through the “focal adhesion” node. Force boundary condition is imposed to this node (and other nodes connected to contracting filaments) and the deformed force-balanced network configuration is obtained as described in Sec. II.B. The length d' of the filament connecting the center cell and the displaced node is then computed. We then consider the contraction of this filament generates a displacement component for the cell center, i.e.,

$$\delta \mathbf{x} = \max\{\delta l - (d - d'), 0\} \cdot \mathbf{d}'_0 \quad (4)$$

where δl is intrinsic contraction of the filament, d and d' are respectively the distance between the cell center and the adhesion node before and after ECM deformation due to filament contraction, and \mathbf{d}'_0 is the unitary direction vector along the filament direction after ECM deformation.

- (iii) Once the displacement components associated with all filaments are computed, the center of mass position of the cell is updated as follows (see Fig. 3(d)):

$$\mathbf{x}_{t+1} = \mathbf{x}_t + \sum_i \delta \mathbf{x}_i \quad (5)$$

where the sum is taken for all filaments, and $\delta \mathbf{x}_i$ is the displacement component associated with the i th filament. The persistent direction \mathbf{n}_0 is updated as the direction of the cell displacement (i.e., $\sum_i \delta \mathbf{x}_i$). We note that Eq. (4) and Eq. (5) imply that cell locomotion is due to actin filament contraction and depends on the stiffness of the local ECM.

- (iv) All of the current adhesion sites are checked and those reach their life span T_a are consider to break, leading to the detachment of the cell surface from the collagen fibers.

In the simulation, time is discretized such that a migration cycle is completed during the elapsing of one time step dt . The life time of focal adhesion sites $T_a = 2dt$, which is calibrated based on the experimental data (see Sec. IV for details). Once an entire migration cycle is completed, the position of cytoplasm sphere (and thus, the center of mass of the cell) is updated and the cell starts the next migration cycle, by repeating the steps (i) to (iv).

We also note that the cell-cell contact adhesion is not explicitly considered in this model, since our focus here is highly motile breast cancer cells with very weak cell-cell adhesion. In addition, we employ a minimal model for the contact inhibition effect for multi-cellular systems. In particular, we consider that if a pair of cells with radius R_s ($\sim 10\mu m$) overlap, they feel a mutual repulsive force proportional to the linear overlap distance, i.e., $F_r = \kappa \delta R$, where κ is an effective elastic constant depending on the modulus of the cell, $\delta R = 2R_s - d_s$ is the overlap distance, and d_s is the cell center separation distance. In the subsequent sections, we will validate our model using single-cell migration experiments and employ the model to predict multi-cell migration dynamics.

IV. SINGLE-CELL MIGRATION DYNAMICS

In this section, we employ our model to investigate single cell migration dynamics and its regulation by the microstructure and mechanical properties of the micro-environment (i.e., the ECM network). We mainly focus on MCF-10A breast cancer cells in our simulations. The MCF-10A cell are highly motile non-metastatic cancer cells which exhibit strong micro-mechanical coupling of ECM networks when moving on collagen gels and do not degrade the collagen fibers [66]. Therefore, this system provides an ideal system for testing our model. In the fol-

lowing discussions, we will directly use the experimental results to validate our model predictions. The experimental details are provided in Ref. [66].

A. Migration dynamics of MCF-10A cells on isotropic collagen gel

We first employ our model to study the migration dynamics of individual MCF-10A breast cancer cells on isotropic collagen gels with randomly oriented fibers. It is well established that in the case, the overall cell dynamics can be captured by the active-particle model [67], i.e.,

$$\gamma d\mathbf{r}/dt = F\hat{\mathbf{e}} + \xi \quad (6)$$

where \mathbf{r} is the particle center of mass, γ is an effective friction coefficient, F is an effective constant self-propelling force, $\hat{\mathbf{e}}$ is the persistent direction which is subject to a random rotational diffusion and ξ is a white-noise random displacement (MSD) σ^2 is given by [67]

$$\sigma^2(t) = [4D + 2v^2\tau_R]t + 2v^2\tau_R^2[e^{-t/\tau_R} - 1] \quad (7)$$

where D is the diffusivity of the particle, v is the persistent velocity and τ_R is the relaxation time for rotation diffusion of the persistent direction. It can be seen from Eq. (7) that for small t , the particle exhibit ballistic dynamics with $\sigma^2 \propto t^2$. At large t , the system is diffusive, with $\sigma^2 \propto t$.

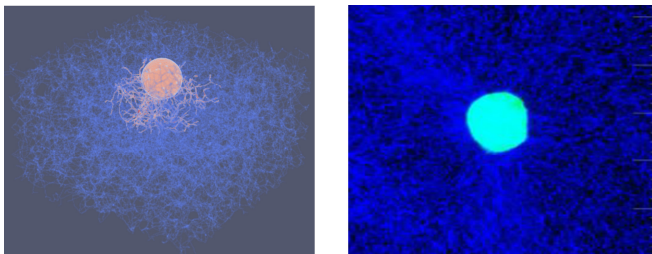


FIG. 4: Left panel: 3D visualization of a single MCF-10A cell migrating on isotropic collagen gel with randomly oriented fibers. The contraction of the actin filaments generates active tensile forces, which are transmitted to the collagen fibers (shown in red or dark gray in print version). Right panel: Confocal microscopy image of a migrating MCF-10A cell (bright blue) on collagen gel. The collagen fibers are shown in dark blue (or dark gray in print version). The linear size of the system is $\sim 100\mu\text{m}$.

Figure 4 shows the 3D visualization of a single MCF-10A migrating on isotropic collagen gel with randomly oriented fibers (see the left panel). The 3D collagen network model is obtained via stochastic reconstruction based on the structural statistics extracted from confocal images, as described in Sec. IIA. The contraction of the actin filaments generates active tensile forces, which are transmitted to the collagen fibers and propagate in the

ECM network. The fibers carrying large tensile forces are highlighted in red color. The right panel of the figure shows a confocal microscopy image of a migrating MCF-10A cell (bright blue) on isotropic collagen gel. It can be seen that the collagen fibers in the vicinity of the cell surface tend to orient perpendicularly to the cell surface, implying that the cell generates traction forces and pulls the fibers, consistent with the simulation results.

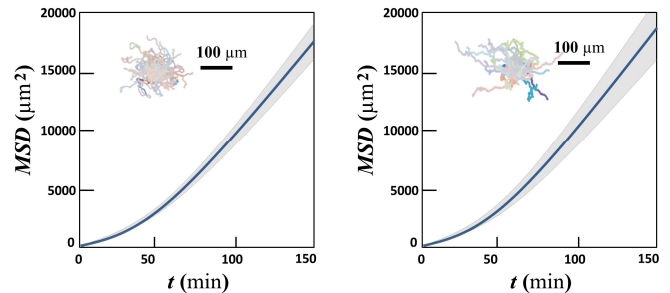


FIG. 5: Comparison of the mean square displacement (MSD) of a single MCF-10A cell migrating on isotropic collagen gel with randomly oriented fibers, respectively obtained from computer simulation (left panel) and *in vitro* experiment (right panel). The insets show the trajectories of the cells.

Figure 5 shows the mean square displacement (MSD) of a single MCF-10A cell migrating on isotropic collagen gel with randomly oriented fibers, respectively obtained from computer simulation (left panel) and *in vitro* experiment (right panel). The initial ballistic dynamics (i.e., $\sigma^2 \propto t^2$) can be clearly seen, which is followed by the diffusive dynamics (i.e., $\sigma^2 \propto Dt$). The cell diffusivity obtained from the simulations and experiments are respectively $D \approx 94\mu\text{m}^2/\text{min}$ and $D \approx 103\mu\text{m}^2/\text{min}$, which agree well with one another. The insets of Fig. 5 show the trajectories of an ensemble of cells respectively obtained from the simulations and experiments. It can be clearly seen that the cell migration is isotropic, as expected for a cell in a homogeneous micro-environment without any externally applied cues. These results clearly indicate the validity of our model.

B. Migration dynamics of MCF-10A cells on collagen gel with aligned fibers

With our model validated by experiments, we now employ it to study cell migration in complex micro-environment, such as collagen gels with aligned fibers, which are difficult to fabricate experimentally. The 3D virtual ECM networks are stochastic constructed by maximizing the fiber orientation metric Ω along the x-direction (see Sec. IIA for details). This leads to model networks with fibers mainly aligned along the x-direction (see Fig. 6).

Figure 6 shows a typical trajectory of a MCF-10A cell migrating on 3D collagen gel with horizontally aligned

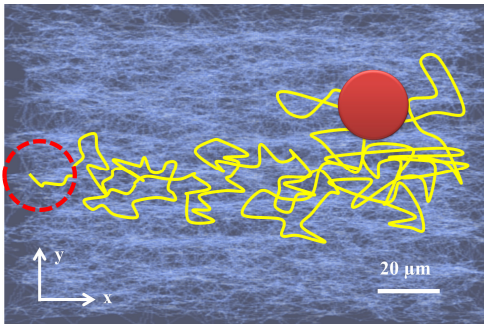


FIG. 6: A typical trajectory of MCF-10A cell migrating on 3D collagen gel with horizontally aligned fibers obtained from simulations.

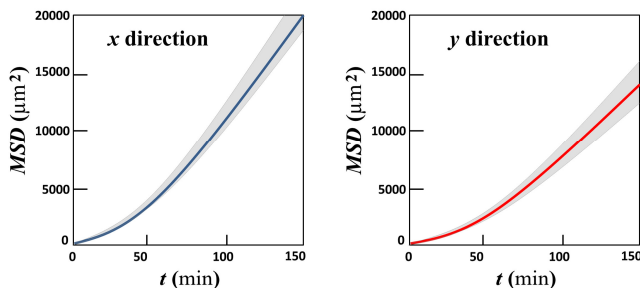


FIG. 7: Mean squared displacement (MSD) of MCF-10A cell migrating on 3D collagen gel with horizontally aligned fibers (along the x-direction) respectively along the x-direction (left panel) and y-direction (right panel). Anisotropy in migration can be clearly observed, i.e., the cell tends to move along the direction of fiber aligned, a phenomenon known as contact guidance.

fibers obtained from simulations. It can be clearly seen that the cell tends to migrate along the direction consistent with the fiber alignment direction (e.g., in this case, x-direction). This can also be seen quantitatively seen from the MSD analysis. Figure 7 shows the MSD of the migrating cell respectively along the x-direction (left panel) and y-direction (right panel). Anisotropy in the migration can be clearly observed, i.e., the cell moves much faster long the fiber alignment direction than the perpendicular direction.

We note that the phenomenon that cells tend to migrate along the fiber alignment direction is well known and termed as “contact guidance” [12, 13]. In our simulations, as the migrating cell pulls the ECM fibers, the large tensile forces are mainly carried by chains of aligned fibers, which are typically referred to as “force chains” [34, 54]. The high-stress fibers on the force chains are effective stiffer (e.g., due to strain hardening) and thus, can support large-magnitude locomotion steps along chain directions, and in this case, the fiber alignment direction.

C. Migration dynamics of MCF-10A cells on collagen gel with a stiffness gradient

We now employ our model to study cell migration dynamics on collagen gels with a stiffness gradient. As described in Sec. IIA, the structural model of the 3D ECM is constructed based on the experimentally obtained statistics of a 2 mg/ml collagen gel with randomly oriented fibers. Once the 3D structural model is obtained, a linear stiffness distribution a long x-direction with a constant gradient is built. This is achieved by re-scaling the Young’s modulus of the fiber according to $E(x) = E \cdot (1 + x/L)$, where x is the x-coordinate of the center of the fiber.

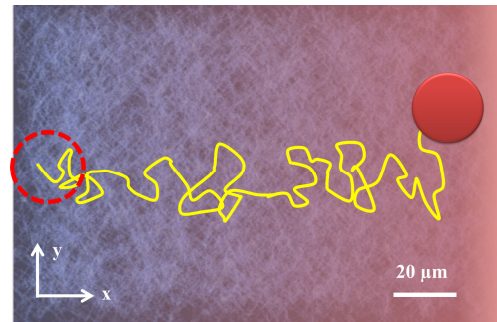


FIG. 8: A typical trajectory of MCF-10A cell migrating on 3D collagen gel with a stiffness gradient along the x-direction obtained from simulations.

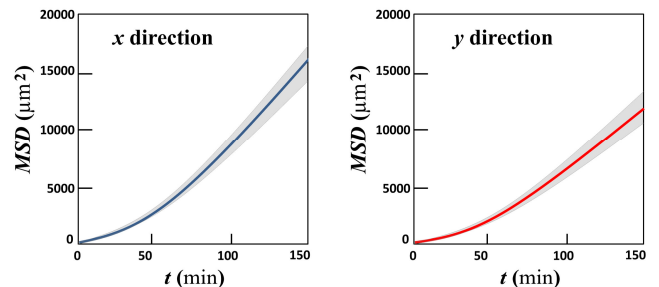


FIG. 9: Mean squared displacement (MSD) of MCF-10A cell migrating on 3D collagen gel with a stiffness gradient (along the x-direction), respectively along the x-direction (left panel) and y-direction (right panel). Anisotropy in migration can be clearly observed, i.e., the cell tends to move up against the stiffness gradient, a phenomenon known as durotaxis.

Figure 8 shows a typical trajectory of a MCF-10A cell migrating on 3D collagen gel with a stiffness gradient along the x-direction. Similar to the case of contact guidance, it can be clearly seen that the cell tends to migrate along the direction against the stiffness gradient along the positive x-direction. This can also be seen quantitatively seen from the MSD analysis. Figure 9 shows the MSD of the migrating cell respectively along the x-direction (left panel) and y-direction (right panel).

Anisotropy in the migration can be clearly observed, i.e., the cell moves much faster along the stiffness gradient direction than the perpendicular direction. We note that an important distinction between migration anisotropy in this case and the contact guidance case is that here the cell migration is uni-directional, i.e., up the stiffness gradient; while in the contact guidance case, the migration is bi-directional, i.e., along the fiber alignment direction but the cells can go in both ways.

The phenomenon that cells migrate against stiffness gradient of the ECM is well known and termed as “durotaxis” [8–10]. In our simulations, as the migrating cell pulls the ECM fibers, the stiffer fibers will possess smaller deformation, which in turn leads to larger locomotion components towards these fibers (c.f. Eq.(4)). The accumulated effect of many local migration steps is the overall biased migration up the stiffness gradient as observed in the experiments.

V. STRONGLY CORRELATED MULTI-CELLULAR DYNAMICS

In Sec. IV, we show that our computational model can capture the salient features of single-cell migration dynamics in both homogeneous and complex micro-environment. In this section, we employ the model to investigate multi-cellular migration dynamics. As mentioned in Sec. III, we do not explicitly model cell-cell adhesion here (due to the weak adhesion between the cancer cells) and use a minimal model for cell-cell repulsion due to contact inhibition (see Sec. III for details). In addition, in this study, we focus on relatively small system, containing ~ 20 cells.

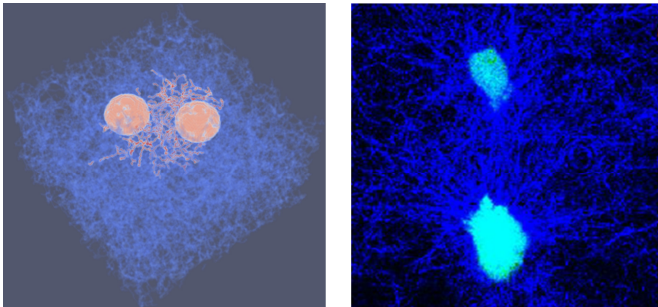


FIG. 10: Left panel: 3D visualization of two closely spaced MCF-10A cells migrating on isotropic collagen gel with randomly oriented fibers. The collagen fibers carrying large tensile forces generated by actin filament contraction are highlighted in red. Right panel: Confocal microscopy image of a pair of migrating MCF-10A cells (bright blue) on collagen gel. The collagen fibers are shown in dark blue (or dark gray in print version).

Figure 10(a) shows 3D visualization of a small portion (with a linear size $\sim 50\mu m$) of the simulation box which contains two closely spaced MCF-10A cells mi-

grating on isotropic collagen gel with randomly oriented fibers. The active tensile forces generated by the cells (due to actin filament contraction) are transmitted to the collagen fibers. The collagen fibers carrying large tensile forces are highlighted in red. Figure 10(a) shows the confocal microscopy image of a pair of migrating MCF-10A cells (bright blue) on collagen gel. It can be clearly seen that the collagen fibers (dark blue) between the two cells form a mesoscopic scale structure, which is clearly distinguished from original homogeneous ECM network and is consistent with the meso-scale structure formed by the high-stress fibers in our simulations.

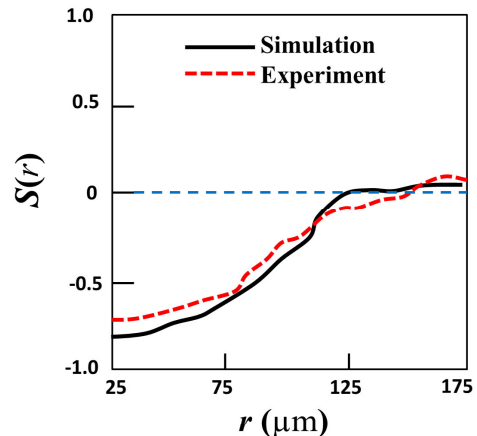


FIG. 11: Comparison of the velocity correlation function $S(r)$ (see the text for definition) of MCF-10A cells migrating on isotropic collagen gel with randomly oriented fibers, respectively obtained from computer simulation (solid curve) and *in vitro* experiment (dashed curve).

To quantify the correlations in the collective migration dynamics of multiple MCF-10A cells, we employ the velocity correlation function $S(r)$, i.e.,

$$S(r) = \langle \mathbf{v}_i(\mathbf{x}) \cdot \mathbf{v}_j(\mathbf{x} + \mathbf{r}) \rangle / (|\mathbf{v}_i(\mathbf{x})| |\mathbf{v}_j(\mathbf{x} + \mathbf{r})|) \quad (8)$$

where $r = |\mathbf{r}|$, i, j denote a pair of cells connected by the remodeled meso-scale ECM structures and \langle, \rangle denotes ensemble average over all different cell pairs. We note that in computing $S(r)$, we only consider a subsets of cell pairs, i.e., those between which the meso-scale structures are formed. This allows us to clearly obtain the effects of such meso-structure on the collective dynamics of the cells, if any. Due to cell’s mutual exclusion effects, $S(r) = 0$ for $r < D^*$ and D^* is roughly the diameter of a cell. In addition, two cells separated by very large distances are not correlated, i.e., $S(r) \approx 0$ for large r values. A positive $S(r)$ indicates that the cells tend to move in the same direction, implying a net “flow” of cells in the system. On the other hand, a negative $S(r)$ indicates that the cells move towards one another, implying the formation of aggregation or clusters.

Figure 11 shows the velocity correlation function $S(r)$ of MCF-10A cells migrating on isotropic collagen gel

with randomly oriented fibers, respectively obtained from computer simulation (solid curve) and *in vitro* experiment (dashed curve). It can be seen that the simulation results agree very well with experimental data. Interestingly, the $S(r)$ functions (beyond the trivial exclusion region) start from a very negative value (close to the minimal value -1) around $D^* \approx 25\mu m$, slowly increase to zero and then fluctuate around zero. This indicates the cells tend to move towards one another, facilitated by the mesoscopic structures of the remodeled ECM, which is also confirmed by time-lapse confocal data [66].

Our results indicate that strongly correlated cell migration dynamics is correlated with the meso-scale ECM structures due to cell remodeling. One possible reason is that the meso-structures are composed of many force chains (or a “force network”), which are in turn composed of fibers carrying large tensile forces. Therefore, the fibers in the meso-structures (at least in our simulations) are stiffer than the remaining stress-free fibers, which indicates that the meso-structures themselves are stiffer than the surrounding ECM. These stiffer meso-structures can then facilitate correlated cell migration via durotaxis, and also facilitate indirect mechanical coupling between the migrating cells.

VI. CONCLUSIONS AND DISCUSSION

In this paper, we develop a computational model for cell migration in complex micro-environment, which explicitly takes into account a variety of cellular level processes including focal adhesion formation and disassembly, active traction force generation and cell locomotion due to actin filament contraction, transmission and propagation of tensile forces in the ECM. We employ statistical descriptors obtainable from confocal imaging to quantify and control the 3D ECM network microstructure and use a nonlinear mechanical model for the ECM networks, which incorporates buckling of collagen fibers upon compression and strain-hardening upon stretching. We validate our model by accurately reproducing single-cell dynamics of MCF-10A breast cancer cells migrating on collagen gels and show that the durotaxis and contact guidance effects naturally arise as a consequence of

the cell-ECM micro-mechanical interactions considered in the model. Moreover, our model predicts strongly correlated multi-cellular migration dynamics, which are resulted from the ECM-mediated mechanical coupling among the migrating cell and are subsequently verified in *in vitro* experiments using MCF-10A cells.

Although focusing on the non-metastatic MCF-10A breast cancer cells migrating on 3D collagen gels, our model can be generalized to investigate the migration of mesenchymal cells (e.g., invasive MDA-MB-231 breast cancer cells) in 3D ECM. The key modification is to explicitly model ECM degradation by the cells, which can be achieved using the following rule: A migrating cell degrades collagen fibers with a probability $p_b \propto \exp(-r)$, with r the distance from the fiber to the cell membrane. A degraded fiber is removed from the network in subsequent simulation steps. In addition, cell-cell adhesion can also be easily incorporated into the model to investigate a wide range of cell lines with different phenotypes. With proper modifications and generalizations, as well as efficient parallel implementation, it is expected that the model could be employed to investigate collective migratory behaviors and emergent self-organizing multi-cellular patterns resulted from ECM-mediated mechanical signaling among the cells.

Acknowledgments

Y. Z., H. N. and Y. J. thank Arizona State University for the generous start-up funds and the University Graduate Fellowships. Q. F., X. W., and F. Y. thank the Chinese Academy of Sciences (CAS), the Key Research Program of Frontier Sciences of CAS (Grant No. QYZDB-SW-SYS003). L. L. and R. L. thank the National Natural Science Foundation of China (Grants No. 11474345, No. 11674043, No. 11604030, and No. 11774394). B. S. thank the support from the Scialog Program sponsored jointly by Research Corporation for Science Advancement and the Gordon and Betty Moore Foundation. B. S. is partially supported by the Medical Research Foundation of Oregon and SciRIS-II award from Oregon State University and by the National Science Foundation Grant PHY-1400968.

-
- [1] A. Aman, and T. Piotrowski, Cell migration during morphogenesis. *Developmental Biology* **341**, 20-33 (2010)
 - [2] P. Friedl, and D. Gilmour, Collective cell migration in morphogenesis, regeneration and cancer. *Nature Reviews Molecular Cell Biology* **10**, 445 (2009).
 - [3] A. Vaezi, C. Bauer, V. Vasioukhin, and E. Fuchs, Actin cable dynamics and Rho/Rock orchestrate a polarized cytoskeletal architecture in the early steps of assembling a stratified epithelium. *Developmental Cell* **3**, 367-381 (2002).
 - [4] S. Werner, T. Krieg, and H. Smola, Keratinocytefibroblast interactions in wound healing. *Journal of Investigative Dermatology* **127**, 998-1008 (2007).
 - [5] A. J. Ridley, M.A. Schwartz, K. Burridge, R.A. Firtel, M.H. Ginsberg, G. Borisy, J.T. Parsons, and A.R. Horwitz, Cell migration: integrating signals from front to back. *Science* **302**, 1704-1709 (2003).
 - [6] P. Friedl, and E.-B. Brocker, The biology of cell locomotion within three-dimensional extracellular matrix. *Cellular and Molecular Life Sciences CMLS* **57**, 41-64 (2000).
 - [7] H. Szurmant, and G.W. Ordal, Diversity in chemotaxis mechanisms among the bacteria and archaea. *Microbiol-*

- ogy and Molecular Biology Reviews **68**, 301-319 (2004).
- [8] S. V. Plotnikov, A.M. Pasapera, B. Sabass, and C.M. Waterman, Force fluctuations within focal adhesions mediate ECM-rigidity sensing to guide directed cell migration. *Cell* **151**, 1513-1527 (2012).
- [9] R. Sunyer, V. Conte, J. Escribano, A. Elosegui-Artola, A. Labernadie, L. Valon, D. Navajas, J.M. Garca-Aznar, J.J. Munoz, and P. Roca-Cusachs, Collective cell durotaxis emerges from long-range intercellular force transmission. *Science* **353**, 1157-1161 (2016).
- [10] E. Hadjipanayi, V. Mudera, and R. A. Brown, Guiding cell migration in 3D: a collagen matrix with graded directional stiffness. *Cell Motil. Cytoskeleton* **66** 121-8 (2009).
- [11] S. B. Carter, Haptotaxis and the mechanism of cell motility. *Nature* **213**, 256 (1967).
- [12] P. P. Provenzano, D.R. Inman, K.W. Eliceiri, S.M. Trier, and P.J. Keely, Contact guidance mediated three-dimensional cell migration is regulated by Rho/ROCK-dependent matrix reorganization. *Biophysical Journal* **95**, 5374-5384 (2008).
- [13] J. H. Wang, and E.S. Grood, The strain magnitude and contact guidance determine orientation response of fibroblasts to cyclic substrate strains. *Connective Tissue Research* **41**, 29-36 (2000).
- [14] S. Guido and R. T. Tranquillo, A methodology for the systematic and quantitative study of cell contact guidance in oriented collagen gels. Correlation of fibroblast orientation and gel birefringence. *J. Cell Sci.* **105**, 317-31 (1993).
- [15] S. Wang, and P.G. Wolynes, Active contractility in actomyosin networks. *Proceedings of the National Academy of Sciences* **109**, 6446-6451 (2012).
- [16] T. Lecuit, P.-F. Lenne, and E. Munro, Force generation, transmission, and integration during cell and tissue morphogenesis. *Annual Review of Cell and Developmental Biology* **27**, 157-184 (2011).
- [17] M. A. Schwartz, Integrins and extracellular matrix in mechanotransduction. *Cold Spring Harbor perspectives in biology*, a005066 (2010).
- [18] G. Totsukawa, Y. Wu, Y. Sasaki, D.J. Hartshorne, Y. Yamakita, S. Yamashiro, and F. Matsumura, Distinct roles of MLCK and ROCK in the regulation of membrane protrusions and focal adhesion dynamics during cell migration of fibroblasts. *The Journal of Cell Biology* **164**, 427-439 (2004).
- [19] C. A. Jones, M. Cibula, J. Feng, E.A. Krnacik, D.H. McIntyre, H. Levine, and B. Sun, Micromechanics of cellularized biopolymer networks. *Proceedings of the National Academy of Sciences* **112**, E5117-E5122 (2015).
- [20] S. B. Lindstrom, D.A. Vader, A. Kulachenko, and D.A. Weitz, Biopolymer network geometries: characterization, regeneration, and elastic properties. *Physical Review E* **82**, 051905 (2010).
- [21] H. Mohammadi, P.D. Arora, C.A. Simmons, P.A. Janmey, and C.A. McCulloch, Inelastic behaviour of collagen networks in cellmatrix interactions and mechanosensation. *Journal of The Royal Society Interface* **12**, 20141074 (2015).
- [22] S. Nam, K.H. Hu, M.J. Butte, and O. Chaudhuri, Strain-enhanced stress relaxation impacts nonlinear elasticity in collagen gels. *Proceedings of the National Academy of Sciences*, 201523906 (2016).
- [23] Nam, S., J. Lee, D.G. Brownfield, and O. Chaudhuri, Viscoplasticity enables mechanical remodeling of matrix by cells. *Biophysical journal*, 2016. 111(10): p. 2296-2308.
- [24] J. Kim, J. Feng, C.A. Jones, X. Mao, L.M. Sander, H. Levine, and B. Sun, Stress-induced plasticity of dynamic collagen networks. *Nature Communications* **8**, 842 (2017).
- [25] S. Chen, W. Xu, J. Kim, H. Nan, Y. Zheng, B. Sun, and Y. Jiao, Novel inverse finite-element formulation for reconstruction of relative local stiffness in heterogeneous extra-cellular matrix and traction forces on active cells. *Physical Biology* **16**, 036002 (2019).
- [26] A. D. Doyle, N. Carvajal, A. Jin, K. Matsumoto, and K.M. Yamada, Local 3D matrix microenvironment regulates cell migration through spatiotemporal dynamics of contractility-dependent adhesions. *Nature Communications* **6**, 8720 (2015).
- [27] C. Heussinger and E. Frey, Force distributions and force chains in random stiff fiber networks. *Eur. Phys. J. E* **24** 4753 (2007).
- [28] F. Grinnell, and W.M. Petroll, Cell motility and mechanics in three-dimensional collagen matrices. *Annual Review of Cell and Developmental Biology* **26**, 335-361 (2010).
- [29] Y. L. Han, P. Ronceray, G. Xu, A. Malandrino, R.D. Kamm, M. Lenz, C.P. Broedersz, and M. Guo, Cell contraction induces long-ranged stress stiffening in the extracellular matrix. *Proceedings of the National Academy of Sciences* **115**, 4075-4080 (2018).
- [30] X. Ma, M.E. Schickel, M.D. Stevenson, A.L. Sarang-Sieminski, K.J. Gooch, S.N. Ghadiali, and R.T. Hart, Fibers in the extracellular matrix enable long-range stress transmission between cells. *Biophysical Journal* **104**, 1410-1418 (2013).
- [31] P. Ronceray, C.P. Broedersz, and M. Lenz, Fiber networks amplify active stress. *Proceedings of the National Academy of Sciences* **113**, 2827-2832 (2016).
- [32] H. Wang, A. Abhilash, C.S. Chen, R.G. Wells, and V.B. Shenoy, Long-range force transmission in fibrous matrices enabled by tension-driven alignment of fibers. *Biophysical Journal* **107**, 2592-2603 (2014).
- [33] F. Beroz, L.M. Jawerth, S. Munster, D.A. Weitz, C.P. Broedersz, and N.S. Wingreen, Physical limits to biomechanical sensing in disordered fibre networks. *Nature Communications* **8**, 16096 (2017).
- [34] L. Liang, C. Jones, S. Chen, B. Sun, and Y. Jiao, Heterogeneous force network in 3D cellularized collagen networks. *Physical Biology* **13**, 066001 (2016).
- [35] M. H. Zaman, R. D. Kamm, P. Matsudaria, and D. A. Lauffenburger. Computational model for cell migration in three-dimensional matrices. *Biophys. J.* **89**, 1389 (2005).
- [36] A. Vaziri and A. Gopinath. Cell and biomolecular mechanics in silico. *Nature Materials* **7**, 15 (2008).
- [37] P. Masuzzo, M. Van Troys, C. Ampe, and L. Martens, Taking aim at moving targets in computational cell migration. *Trends in cell biology* **26**, 88 (2016).
- [38] F. Ziebert, S. Swaminathan, and I. S. Aranson. Modeling for self-polarization and motility of keratocyte fragments. *J. R. Soc. Interface* **9**, 1084 (2011).
- [39] D. Shao, W. J. Rappel, and H. Levine. Computational model for cell morphodynamics. *Phys. Rev. Lett.* **105**, 108104 (2010).
- [40] D. Shao, H. Levine, and W. J. Rappel. Coupling actin flow, adhesion, and morphology in a computational cell motility model. *Proc. Natl. Acad. Sci. USA* **109**, 6851 (2012).

- [41] U. Z. George, A. Stephanou, and A. Madzvamuse. Mathematical modeling and numerical simulations of actin dynamics in the eukaryotic cell. *J. Math. Biol.* **66**, 547 (2013).
- [42] T. C. Bidone, W. Jung, D. Maruri, C. Borau, R. D. Kamm, and T. Kim, Morphological transformation and force generation of active cytoskeletal networks, *PLoS Comput. Biol.* **13**, e1005277 (2017).
- [43] M. C. Kim, J. Whisler, Y. R., Silberberg, et al. Cell invasion dynamics into a three dimensional extracellular matrix fibre network. *PLoS Comput. Biol.* **11**, e1004535 (2015).
- [44] T. Vicsek, A. Czirok, E. Ben-Jacob, I. Cohen, and O. Shochet, Novel type of phase transition in a system of self-driven particles. *Physical review letters* **75**, 1226 (1995).
- [45] C. Bechinger, R. Di Leonardo, H. Lowen, C. Reichhardt, G. Volpe, Active particles in complex and crowded environments. *Reviews of Modern Physics* **88**, 045006 (2016).
- [46] D. Bi, J. Lopez, J. Schwarz, M. L. Manning, A density-independent rigidity transition in biological tissues, *Nature Physics* **11**, 1074 (2015).
- [47] F. Graner, and J. A. Glazier, Simulation of biological cell sorting using a two-dimensional extended Potts model. *Physical Review Letters* **69**, 2013 (1992).
- [48] Y. Jiao and S. Torquato, Emergent Properties from a Cellular Automaton Model for Invasive Tumor Growth in Heterogeneous Environment, *PLoS Computational Biology* **7**, 1002314 (2011).
- [49] Y. Jiao and S. Torquato, Diversity of Dynamics and Morphologies of Invasive Solid Tumors, *AIP Advances* **2**, 011003 (2012)
- [50] Y. Jiao and S. Torquato, Evolution and Morphology of Microenvironment-Enhanced Malignancy of Three-Dimensional Invasive Solid Tumors, *Physical Review E* **87**, 052707 (2013)
- [51] H. Xie, Y. Jiao, Q. Fan, et. al., Modeling Three-dimensional Invasive Solid Tumor Growth in Heterogeneous Microenvironment under Chemotherapy, *PLoS One* **13**, e0206292 (2018)
- [52] H. Abdel-Rahman, B. Thomas, and T. Kim, A mechanical model for durotactic cell migration, *ACS Biomater Sci Eng* (2019)
- [53] M. Dietrich, H. Le Roy, D. B. Bruckner, H. Engelke, R. Zantl, J. O. Radler and C. P. Broedersz, Guiding 3D cell migration in deformed synthetic hydrogel microstructures, *Soft Matter* **14**, 2816 (2018).
- [54] Nan, H., L. Liang, G. Chen, L. Liu, R. Liu, and Y. Jiao, Realizations of highly heterogeneous collagen networks via stochastic reconstruction for micromechanical analysis of tumor cell invasion. *Physical Review E* **97**, 033311 (2018).
- [55] S. Kirkpatrick, C. D. Gelatt, and M. P. Vecchi, Optimization by simulated annealing. *Science* **220**, 671 (1983).
- [56] D. A. Head, A. J. Levine, and F. C. MacKintosh, Mechanical response of semiflexible networks to localized perturbations. *Phys. Rev. E* **72** 061914 (2005).
- [57] Y. Shokef and S. A. Safran, Scaling laws for the response of nonlinear elastic media with implications for cell mechanics. *Phys. Rev. Lett.* **108**, 178103 (2012).
- [58] J. Steinwachs, C. Metzner, K. Skodzek, et. al. Three-dimensional force microscopy of cells in biopolymer networks. *Nat. Method* **13** 171-6 (2016).
- [59] R. Fernandez-Gonzalez, M. S. Simoes, J. C. Roper, S. Eaton, and J. A. Zallen. Myosin ii dynamics are regulated by tension in intercalating cells. *Dev. Cell* **17**, 736743 (2009).
- [60] T. Lecuit, P. Lenne, and E. Munro. Force generation, transmission and integration during cell and tissue morphogenesis. *Annu. Rev. Cell Dev. Biol.* **27**, 157184 (2011).
- [61] G. Totsukawa, Y. Wu, Y. Sasaki, D. J. Hartshorne, Y. Yamakita, S. Yamashiro, and F. Matsumura. Distinct roles of mlc and rock in the regulation of membrane protrusions and focal adhesion dynamics during cell migration of fibroblasts. *J. Cell Biol.* **164**, 427439 (2004).
- [62] S. K. Boey, D. H. Boal, and D. Discher. Simulations of the erythrocyte cytoskeleton at large deformation. i. microscopic models. *Biophys. J.* **75**, 15731583 (1998).
- [63] D. Discher, D. H. Boal, and S. K. Boey. Simulations of the erythrocyte cytoskeleton at large deformation. ii. micropipette aspiration. *Biophys. J.* **75**, 15841597 (1998).
- [64] M. F. Coughlin and D. Stamenovic. A prestressed cable network model for the adherent cell cytoskeleton. *Biophys. J.* **84**, 13281336 (2003).
- [65] D. Gordon, A. Bernheim-Groswasser, C. Keasar, and O. Farago. Hierarchical self-organization of cytoskeletal active networks. *Phys. Biol.* **9**, 026005 (2012).
- [66] Q. Fan, Y. Zheng, H. Nan, Y. Jiao, and F. Ye, Strongly correlated cell dynamics induced by ECM-mediated long-range mechanical coupling, submitted.
- [67] C. Bechinger, R. D. Leonardo, H. Lowen, C. Reichhardt, G. Volpe and G. Volpe, Active particles in complex and crowded microenvironments, *Rev. Mod. Phys.* **88**, 045006 (2016).